JPE 11-4-21

High-Efficiency Grid-Tied Power Conditioning System for Fuel Cell Power Generation

Jong-Kyou Jeong*, Byung-Moon Han†, Jun-Young Lee*, and Nam-Sup Choi**

†* Dept. of Electrical Engineering, Myongji University, Yongin, Korea
** Div. of Electrical Electronic Communication and Computer Eng., Chonnam National University, Yeosu, Korea

Abstract

This paper proposes a grid-tied power conditioning system for the fuel cell power generation, which consists of a 2-stage DC-DC converter and a 3-phase PWM inverter. The 2-stage DC-DC converter boosts the fuel cell stack voltage of 26-48V up to 400V, using a hard-switching boost converter and a high-frequency unregulated LLC resonant converter. The operation of the proposed power conditioning system was verified through simulations with PSCAD/EMTDC software. Based on the simulation results, a laboratory experimental set-up was built with a 1.2kW PEM fuel-cell stack to verify the feasibility of hardware implementation. The developed power conditioning system shows a high efficiency of 91%, which is a very positive result for the commercialization.

Key Words: DSP (Digital Signal Processor), LLC resonant DC-DC converter, Nernst model, PEM (Proton Exchange Membrane) fuel cell

I. INTRODUCTION

A fuel cell is a clean energy source for generating electricity like a solar cell. Many kinds of fuel cells have been developed for supplying electricity to cars and homes. A PEM fuel cell, which has a simple structure and a high power density, is considered to be a promising DC power source for distributed generation and passenger cars. [1]–[3]

A fuel cell stack shows non-linear characteristics in electrical operation due to the polarization phenomena of the electrochemical reaction. The terminal voltage at the rated load drops to half value at no load. Therefore, the DC-DC converter can boost a low terminal voltage up to a high DC voltage. [4]–[6]

Full-bridge converters, push-pull converters, and boost converters have been widely used as a DC-DC converters for fuel cell stacks. The full-bridge converter has the disadvantage of a high switching loss due to its large number of switching units. The push-pull converter has a lower switching loss due to its lower number of switching units, but it has a rather low efficiency of 88% because it requires a double winding structure on the primary side. The boost converter has a lower switching loss due to its small number of switching units, but it has a lower voltage boosting ratio of 3 to 4 times. Recently, a multi-stage boost converter without a transformer was developed to obtain a high voltage boosting ratio. However, its efficiency is located between 86∼90%. An isolated boost converter was also developed to obtain a high voltage boosting ratio, of which the efficiency is located between 86∼90%. However, it requires large number of switching units and transformers. In order to increase the efficiency and to reduce the number of components, various types of converter have been proposed and are being proposed by many researchers [7]–[11].

This paper proposes a new power conditioning system to interconnect the fuel cell stack with the power grid. The power conditioning system consists of a 2-stage DC-DC converter and a three-phase PWM inverter. The 2-stage DC-DC converter consists of a hard-switching boost converter cascaded with an unregulated LLC resonant converter. The operational feasibility of proposed power conditioning system has been confirmed by computer simulations and the feasibility of the hardware implementation has been verified through experimental results with a laboratory prototype.

II. PROPOSED SYSTEM

Fig. 1 shows the configuration of the proposed power conditioning system including the whole system controller. The power conditioning system for fuel cell power generation requires a high boost-ratio, high efficiency DC-DC converter because fuel cell stacks have a severe voltage variation between the no-load and the full load conditions. In order to satisfy this condition, this paper proposes a new DC-DC converter composed of a conventional boost converter and a 2-stage LLC resonant converter with a high-frequency transformer. The proposed converter has a high efficiency because the LLC converter operates in the soft switching mode with resonance even though the boost converter operates in the hard-switching pattern. It has a simple control structure to

Manuscript received Nov. 27, 2010; revised Mar. 21, 2011
Recommended for publication by Associate Editor Woo-Jin Choi.
† Corresponding Author: erichan@mju.ac.kr
Tel: +82-31-335-6563, Fax: +82-31-330-6816, Myongji University
* Dept. of Electrical Engineering, Myongji University, Korea
** Div. of Electrical Electronic Communication and Computer Eng., Chonnam National University, Korea

regulate an output voltage of up to 400V by controlling the duty ratio of the boost converter. The overall controller for the proposed power conditioning system is divided into the control part for the DC-DC converter and the control part for the grid-tied inverter.

III. Fuel-Cell Modeling

In PEM fuel cells hydrogen gas is supplied to the anode through a platinum catalyst to be ionized into a hydrogen proton and an electron. The hydrogen proton moves to the cathode through a solid polymer membrane and is combined with oxygen supplied to the cathode. Through this electro-chemical reaction, the fuel cell generates electricity and heat, and water as a by-product.

The ideal fuel cell voltage is the same as the equilibrium voltage represented by the Nernst model which is based on Gip's free energy. The actual fuel cell voltage is represented by the reduction characteristic of the equilibrium voltage due to the polarization phenomenon.

The unit cell voltage of the fuel cell is represented by subtracting three polarization losses from the equilibrium voltage with respect to the exchange current density. The unit cell voltage shows non-linear characteristics and is expressed by equation (1).

$$E_{cell} = E_{rev} - E_{act} - E_{con} - E_{ohm} \tag{1}$$

where, E_{rev} is the equilibrium voltage, E_{act} is the activated polarization loss, E_{con} is the concentration polarization loss, and E_{ohm} is the ohmic polarization loss.

The activated polarization loss, which is due to differences in the reaction speed on the electrode, is represented by equation (2).

where, i_o is the exchange current related to the normal and reverse reactions between the electrolyte and the electrode, is represented by equation (3).

The exchange current is dependent on the pressure, the catalyst, the activated energy, and the temperature. If this value is reduced, the activated polarization E_{act} is reduced and the output voltage of the fuel cell E_{cell} is increased. Therefore, the exchange current is a very important parameter in fuel cells.

The concentration polarization loss E_{con} is due to gradient differences in the reaction material concentration, which is represented by equation (4). The ohmic polarization loss E_{ohm}, which is composed of the electrolyte resistance, the electrode resistance, and the lead wire resistance, is represented by equation (5).

$$E_{act} = \frac{RT}{\alpha F} \ln\left(\frac{i + i_{loss}}{i_o}\right) \tag{2}$$

$$i_o = i_o^{ref} a_c L_c \left(\frac{P_r}{P_r^{ref}}\right) \exp\left[-\frac{E_c}{RT}\left(1 - \frac{T}{T_{ref}}\right)\right] \tag{3}$$

$$E_{con} = \frac{RT}{nF} \ln\left(\frac{i_L}{i_L - i}\right) \tag{4}$$

$$E_{ohm} = iR_i. \tag{5}$$

As a result, the output voltage characteristics of fuel cells are represented by the above five equations. If all of the parameters described in these equations are known for a specific fuel cell, its output voltage with respect to the output current can be easily analyzed.

Fig. 2 shows output characteristic curves for a unit cell of a typical fuel cell. The actual cell output voltage E_{cell} is reduced in a non-linear manner by the three polarization components from the equilibrium voltage.

In an actual fuel cell, many unit cells are connected in series as a stack structure to build up the terminal voltage. Therefore, the voltage and current characteristics of the stack are determined by multiplying the unit cell voltage by the number of cells and multiplying the unit cell current density by the area of a cell.

Fig. 3 shows the output voltage characteristic of a fuel cell stack that is composed of 47 cells. The y-axis shows the actual output voltage, while the x-axis shows the fuel cell current. This curve is required to design the DC-DC converter for a fuel cell power conditioning system.

IV. 2-Stage DC-DC Converter

Fig. 4 shows the configuration of the 2-stage DC-DC converter, which is composed of a hard switching boost converter and a soft switching half-bridge LLC resonant converter. The controller is composed of an output voltage sensor, a boost converter control, and a fixed-duty gate pulse generator. The proposed 2-stage DC-DC converter offers several benefits to reduce the complexity of the controller design and to decrease the size of the resonant converter transformer by a high frequency operation over 100kHz. Since each converter has a separate function, it can be designed at the optimal operating point, which helps to increase the overall efficiency.

The input voltage is determined to be 24∼48V by considering the output voltage characteristic of the fuel cell. This voltage is boosted up to 80V by controlling the duty ratio of the boost converter. The half-bridge LLC resonant converter boosts the input voltage of 80V up to 400V by operating a fixed duty ratio.

The control part of the boost converter compares the reference voltage 400V with the measured converter output voltage, and the error signal is passed through the PI control to generate the gate pulse for the boost converter.

When the switch S_b of the boost converter is ON, current flows through the reactor L_b and energy is charged in the reactor. When the switch S_b is OFF, this energy is discharged into the capacitor C_b through the diode D_b.

Fig. 5 shows the four operation modes of the LLC resonant converter, which is composed of two MOSFET switches, a resonant capacitor C_r, the leakage inductance of the transformer L_r and the magnetizing inductance L_m. The secondary side of the transformer is connected to the full-bridge diode rectifier.

Fig. 6 shows the voltage and current waveforms at each component of the LLC resonant converter. The converter operation can be divided into four modes according to the time interval.

- Operation Mode 1 (t_0–t_1)

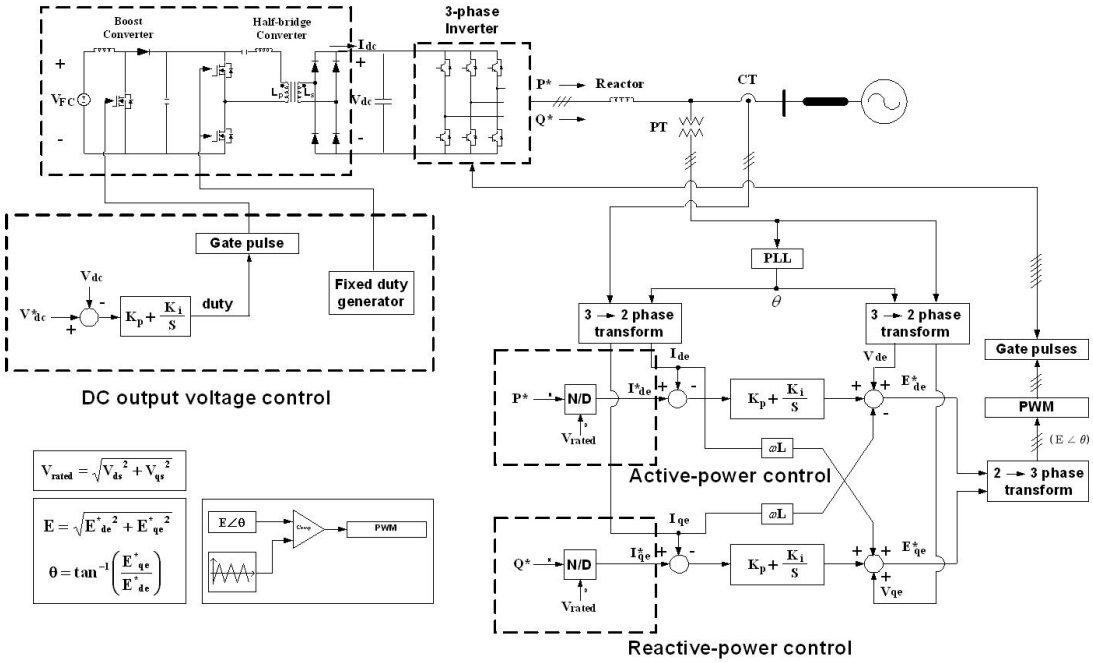

Fig. 1. Configuration of Proposed System.

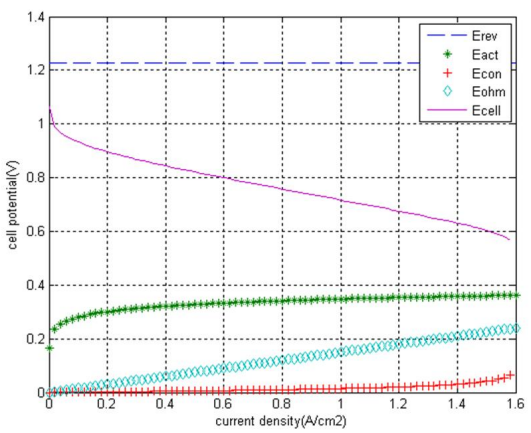

Fig. 2. Output voltage characteristic of Fuel-cell.

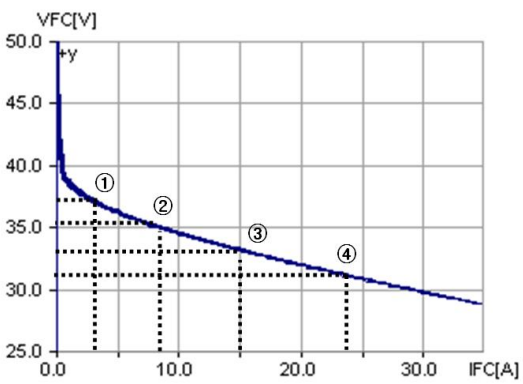

Fig. 3. Output characteristics modeling of fuel cell stack.

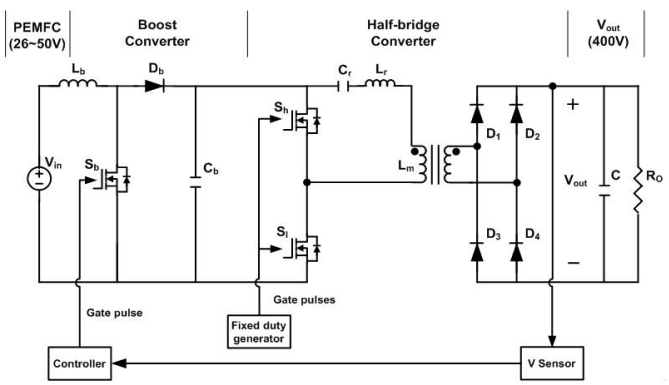

Fig. 4. Circuit Diagram of 2-stage DC-DC Converter.

Fig. 5(a) shows the operation mode in the powering section, which starts at the instant when the MOSFET S_l turns on. The resonant current flows through MOSFET S_l and the energy is transferred to the secondary side of the transformer. The resonant capacitor C_r is charged and the resonant frequency f_r is determined by equation (6), because the magnetizing inductance L_m does not involve in resonance.

$$f_r = \frac{1}{2\pi\sqrt{L_r C_r}}. \tag{6}$$

On the secondary side, diodes D_1 and D_4 are conducting and the current through the magnetizing inductance L_m is linearly increased.

- Operation Mode 2 (t_1–t_2)

Fig. 5(b) shows the operation mode in the dead time section, which starts at the instant when the switch S_l turns off. The current that in used to flow through the switch S_l flows through the diode inside the switch S_h. This allows the zero-voltage switching condition at the switch S_h. In this section the magnetizing current does not increase any more, and the

TABLE I
CIRCUIT PARAMETERS FOR 2-STAGE DC-DC CONVERTER

Input Voltage	25∼50[V]
Output Voltage	400[V]
Output Current	2.5[A]
Switching Frequency	100[kHz]
Resonant Frequency	100[kHz]
Resonant Capacitor	0.8[μF]
Resonant Reactor	2.9[μH]

energy transfer to the secondary side of the transformer is cut off.

- Operation Mode 3 (t_2–t_3)

Fig. 5(c) shows the operation mode in the powering section, which starts at the instant when the switch S_h turns on. The energy that is charged in C_r is transferred to the secondary side of the transformer. On the secondary side, diodes D_2 and D_3 are conducting, and the current through the magnetizing inductance L_m is linearly decreased.

- Operation Mode 4 (t_3–t_4)

Fig. 5(d) shows the operation mode in the dead time section, which starts at the instant when the switch S_h turns off. The current that in used to flow through the switch S_h flows through the diode inside the switch S_l. This allows the zero-voltage switching condition at the switch S_l. In this section the magnetizing current does not increase any more, and the energy transfer to the secondary side of the transformer is cut off.

The switching frequency of the LLC converter f_{sL} is selected to be same as the resonant frequency f_r calculated to reduce the switching loss. The output voltage can be represented by the following equation:

$$\frac{V_o}{V_{in}} = \frac{V_b}{V_{in}} \cdot \frac{V_o}{V_b} = \frac{1}{(1-D)} \cdot \frac{n}{2} \tag{7}$$

where, D means the duty-ratio of the boost converter.

These four operation modes are sequentially repeated according to the switching frequency of 100kHz. Although the switching frequency is rather high, the switching loss is quite small due to the zero-voltage switching scheme.

A hardware prototype of the proposed DC-DC converter was built and tested to verify the application feasibility for fuel cell power generation. The circuit parameters are shown in Table I.

Fig. 7 shows a picture of the proposed DC-DC converter which was built in the lab. The physical size of the DC-DC converter is 150mm×150mm.

Fig. 8 shows the drain-source voltage across each MOSFET in the LLC resonant converter, and the resonant current through the primary winding of the transformer. The switching frequency is fixed at 100kHz, and the LC resonant frequency is also fixed at 100kHz. Through experimental results, it is confirmed that the resonant LLC converter operates properly.

V. DEVICE LOSS ANALYSIS FOR LINK VOLTAGE SELECTION

To select an optimal link voltage, it is necessary to derive a relationship between the link voltage and all of the device losses. To make a guideline to select the link voltage, only the semiconductor device losses will be considered because the

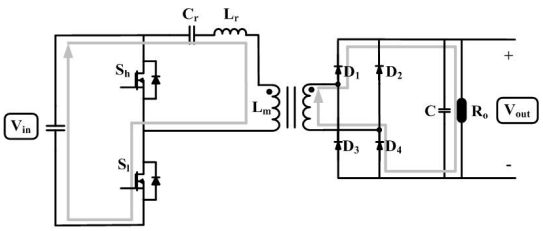

(a) mode 1.

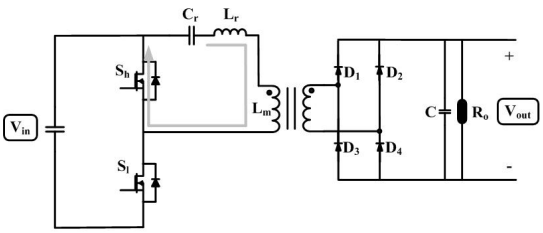

(b) mode 2.

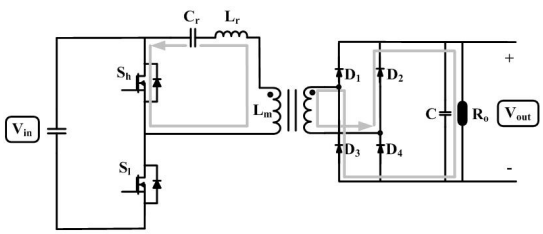

(c) mode 3.

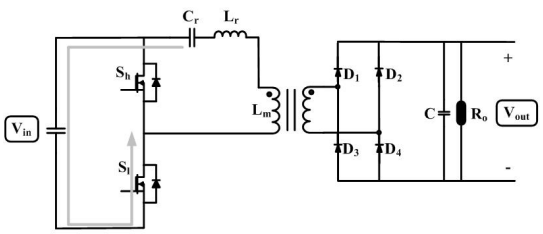

(d) mode 4.

Fig. 5. Operation of LLC Resonant Converter.

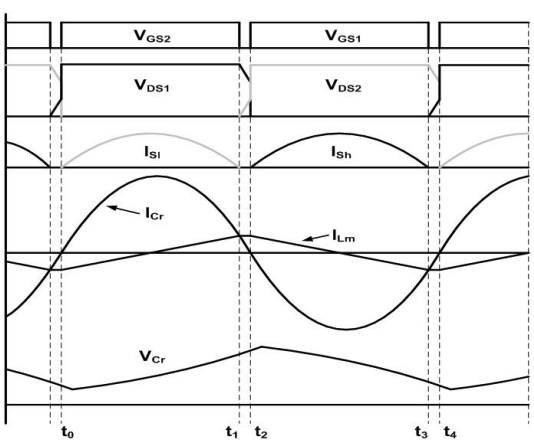

Fig. 6. Operation analysis of LLC Resonant Converter.

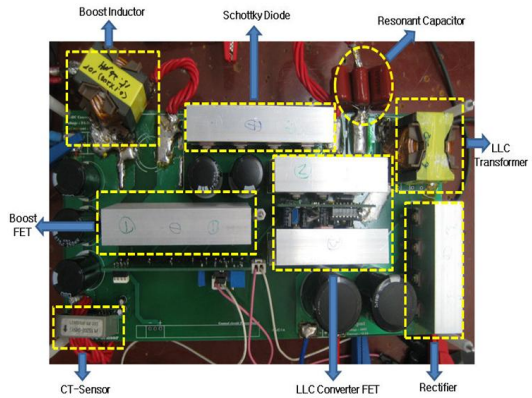

Fig. 7. Picture of proposed DC-DC converter.

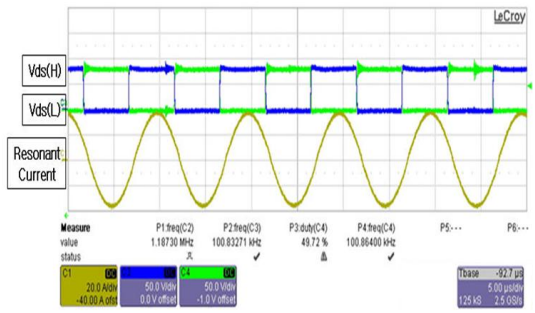

Fig. 8. Drain-source voltage and resonant current of LLC converter.

magnetic element losses become constant if the parameters such as flux swing, wire current density, core material and operational frequency are designed to be identical according to the link voltages. The semiconductor device loss equations can be obtained through the loss analysis of each stage and the procedure is as follows:

- Boost stage loss analysis

Assuming that the boost inductor is large enough to be a current source, the model and its switching waveforms can be depicted as in Fig. 9. After the gate is charged to the threshold voltage V_{th} the MOSFET M_1 is ready to carry current and the gate voltage is rising from V_{th} to the Miller plateau level $V_{gs,miller}$. This is the linear operation level because M_1 operates under the pinch-off state. This state continues until V_{ds1} reaches 0V. During this interval, all of the boost inductor current flows through M_1 because the output diode D_1 changes to the off-state. If the base resistor R_g is small enough for the gate drive transistor to be operated in the saturation region, the turn-on gate current $I_{g,on}$ can be written as:

$$I_{g,on} = \frac{V_{CC} - V_{CE,sat} - V_{gs,miller}}{R_g} \tag{8}$$

where $V_{CE,sat}$ is the collector-emitter saturation voltage of the NPN transistor Q_1 and V_{CC} is the gate drive voltage. $V_{gs,miller}$ can be obtained from the transfer characteristics of M_1 and a method is explained to calculate $V_{gs,miller}$ from the I_D-V_{gs} curves of MOSFETs in [13]. The turn-on gate current determines the turn-on time of M_1 $T_{on,B}$ and it can be calculated as:

$$T_{on,B} = \frac{Q_{gd}}{I_{g,on}}. \tag{9}$$

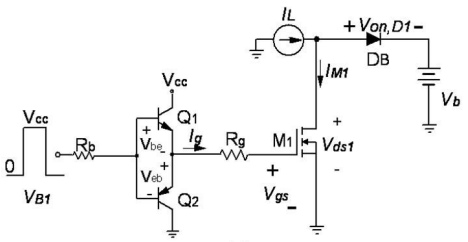

(a)

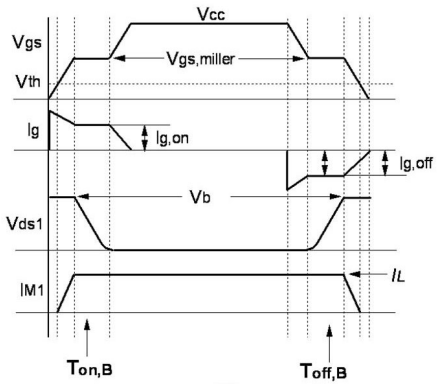

(b)

Fig. 9. Boost converter model(a) and its switching waveform(b) for loss analysis.

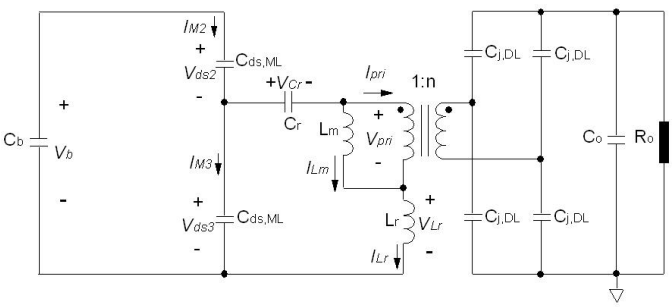

Fig. 10. Equivalent circuit of LLC converter during dead-times.

Thus the turn-on switching loss of the boost converter can be written as follows:

$$P_{on,M1} = \frac{1}{2} I_L (V_b - V_{on,D1}) T_{on,B} f_{sB} \tag{10}$$

where $V_{on,D1}$ is the on-drop voltage of D_1 and f_{sB} is the switching frequency of the boost converter. After V_{ds1} reaches 0V, the gate voltage increases to the final gate drive voltage and M_1 becomes completely turned on.

When the gate-source voltage is discharged to the Miller plateau level, M_1 enters the linear operation region and the turn-off gate current $I_{g,off}$ becomes:

$$I_{g,off} = \frac{V_{EC,sat} - V_{gs,miller}}{R_g}. \tag{11}$$

In this equation, $V_{EC,sat}$ is the emitter-collector saturation voltage of the PNP transistor Q_2. This current charges the drain-source capacitance of M_1 and the turn-off time of M_1 $T_{off,B}$ is determined as follows:

$$T_{off,B} = \frac{Q_{gd}}{I_{g,off}}. \tag{12}$$

TABLE II
LOSS EQUATIONS FOR LINK VOLTAGE SELECTION

	Loss equation
Boost FET loss	$\frac{1}{2}I_L(V_b - V_{on,D1})(T_{on,B} + T_{off,B})f_{sB} + C_{ds,M1}V_b^2 f_{sB} + \left(\frac{P_o^2}{V_{in}^2}\frac{V_b - V_{in}}{V_b}\right)R_{ds,M1}$
Boost diode loss	$C_{j,D1}V_b^2 f_{sB} + \frac{P_o V_{on,D1}}{V_b}$
LLC FET loss	$\frac{1}{3}V_b\left(\frac{V_o}{4nL_m f_{sL}} - C_{ds,ML}\frac{V_b}{T_{off,L}}\right)T_{off,L}f_{sL} + \left(\frac{2P_o}{V_b}\sqrt{\frac{R_o^2}{32n^4L_m^2 f_{sL}^2} + \frac{\pi^2}{8}}\right)^2 R_{ds,ML}$
LLC output rectifier loss	$\frac{2P_o}{V_o}V_{on,DL}$

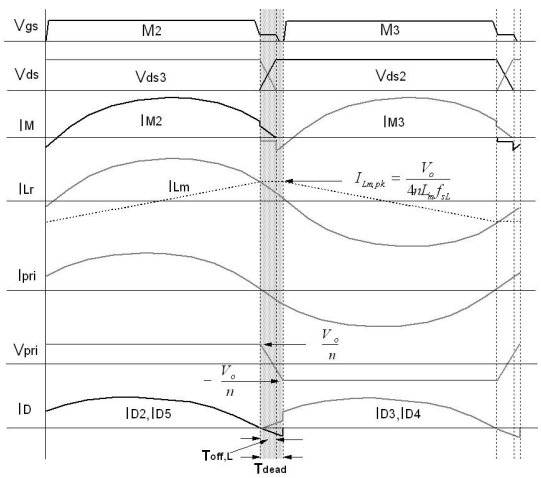

Fig. 11. Switching waveform of the unregulated LLC converter.

Therefore, the turn-off switching loss of the boost converter is:

$$P_{off,M1} = \frac{1}{2}I_L(V_b - V_{on,D1})T_{off,B}f_{sB} \tag{13}$$

Besides theses losses, there is a switching loss due to the drain-source capacitance of M_1 $C_{ds,M1}$ and the junction capacitance of D_1 $Cj,D1$, and it can be written as:

$$P_C = (C_{ds,M1} + C_{j,D1})V_b^2 f_{sB}. \tag{14}$$

The conduction losses of M_1 and D_1 can be calculated using the RMS and the average current carried by them, and they can be calculated as follows:

$$P_{con,M1} = \left(\frac{P_o^2}{V_{in}^2}\frac{V_b - V_{in}}{V_b}\right)R_{ds,M1} \tag{15}$$

$$P_{cond,D1} = \frac{P_o V_{on,D1}}{V_b} \tag{16}$$

where $R_{ds,M1}$ is the on-resistance of M_1. Therefore, the total device loss of the boost converter is as follows:

$$P_{Boost} = P_{on,M1} + P_{off,M1} + P_C + P_{con,M1} + P_{con,D1}. \tag{17}$$

- LLC stage loss analysis

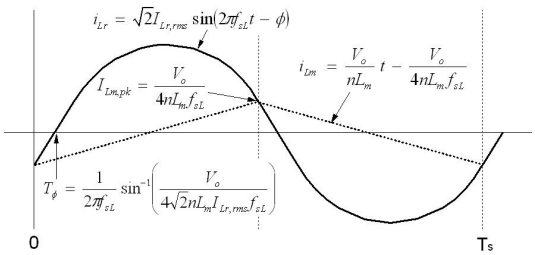

Fig. 12. Resonant current waveform and its key expressions.

Before the loss analysis is carried out, it is necessary to determine L_m to achieve the soft-switching condition. Assuming that the reverse recovery time of the output rectifier is negligible, the equivalent circuit during the dead-time T_{dead} can be depicted as in Fig. 10. To achieve the ZVS condition when $f_{sL} = f_r$, the peak magnetizing current $I_{Lm,pk}$ should be large enough to discharge the output capacitances of the MOSFETs and the junction capacitances of the output rectifiers $D_2 \sim D_5$ during T_{dead}. This condition gives the design guideline of L_m, and it is written as:

$$L_m \le \frac{V_o T_{dead}}{4n(2C_{ds,ML} + 4n^2 C_{j,DL})V_b f_{sL}} \tag{18}$$

where $C_{j,DL}$ is the junction capacitance of each diode in the output rectifier and $C_{ds,ML}$ is the drain-source capacitance of M_2 or M_3. Eq. (18) guarantees the ZVS condition of the switches and the loss analysis is performed with the assumption that L_m is designed to meet this inequality. Fig. 11 depicts the switching waveform of an unregulated LLC converter. When M_2 enters the turn-off transition, it experiences the linear operation region while the gate pulse passes through the Miller plateau level and V_{ds2} is linearly increased. Because the slope of V_{ds2} determines that of V_{ds3}, the discharging current of the drain-source capacitance of M_3 can be calculated as:

$$I_{M3} = -C_{ds,ML}\frac{V_b}{T_{off,L}}. \tag{19}$$

The turn-off time of M_2 $T_{off,L}$ can be calculated with eq. (12). Therefore, the current flowing through the channel of

M_2 can be obtained as:

$$I_{M2} = I_{Lr} + I_{M3} = I_{Lm,pk} + I_{M3} = \frac{V_o}{4nL_m f_{sL}} - C_{ds,ML}\frac{V_b}{T_{off,L}}. \quad (20)$$

With this equation, the switching loss of M_2 can be written as eq. (21) by assuming that i_{Lr} is linearly decreased during the dead-time.

$$P_{off,M2} = \frac{1}{6}V_b\left(\frac{V_o}{4nL_m f_{sL}} - C_{ds,ML}\frac{V_b}{T_{off,L}}\right)T_{off,L}f_{sL}. \quad (21)$$

The same turn-off loss happens at M_3, and so the total turn-off loss of the MOSFETs can be found as follows:

$$P_{off,SW} = \frac{1}{3}V_b\left(\frac{V_o}{4nL_m f_{sL}} - C_{ds,ML}\frac{V_b}{T_{off,L}}\right)T_{off,L}f_{sL} \quad (22)$$

Because M_2 and M_3 exhibit the ZVS operation, eq. (22) produces the total switching loss of the MOSFETs. Fig. 12 is the resonant current waveform and its key expressions. The difference between the resonant current and the magnetizing current is transferred to the load and it can be expressed as:

$$\frac{2f_{sL}}{n}\int_0^{1/(2f_{sL})}(i_{Lr} - i_m)\,dt = \frac{V_o}{R_o}. \quad (23)$$

With eq. (23) and the expressions of i_{Lr} and i_{Lm} in Fig. 12, the RMS value of the resonant current can be obtained as follows:

$$I_{Lr,rms} = \frac{2P_o}{V_b}\sqrt{\frac{R_o^2}{32n^4L_m^2f_{sL}^2} + \frac{\pi^2}{8}}. \quad (24)$$

Accordingly, the total conduction loss of M_2 and M_3 can be calculated as:

$$P_{con,SW} = \left(\frac{2P_o}{V_b}\sqrt{\frac{R_o^2}{32n^4L_m^2f_{sL}^2} + \frac{\pi^2}{8}}\right)^2 R_{ds,ML} \quad (25)$$

where $R_{ds,ML}$ is the on-resistance of M_2 or M_3. Because the output rectifier has only a conduction loss due to the ZVZCS operation, its loss expression can be written as eq. (26).

$$P_{con,REC} = \frac{2P_o}{V_o}V_{on,DL} \quad (26)$$

where $V_{on,DL}$ is the on-drop voltage of each diode in the output rectifier. Therefore, the total device loss of the LLC converter is:

$$P_{loss,LLC} = P_{off,SW} + P_{con,SW} + P_{con,REC}. \quad (27)$$

The loss equations to select the link voltage are rearranged in Table II. Performing the partial derivative of these loss equations with respect to V_b, the optimal link voltage $V_{b,opt}$ can be obtained with the selected device parameters. Based on the calculated value of $V_{b,opt}$ some adjustment should be performed considering the device voltage-ratings and the power losses.

TABLE III
NEXA POWER MODULE

Rated net power	1200 [W]
DC voltage range	25 ~ 50 [V]
DC current range	0 ~ 48 [A]
Rated DC voltage	26 [V]
Rated DC current	46 [A]

TABLE IV
OPERATION SCENARIO FOR COMPUTER SIMULATION

Time [s]	1 ①	2 ②	3 ③	4 ④	5	6	7	8
P [W]	100	300	500	1000	1000	500	300	100
Q [Var]	0	300	100	0	0	300	100	0

VI. COMPUTER SIMULATION

In order to analyze the operation of the proposed fuel-cell power conditioning system, first the modeling of the fuel-cell was carried out. The electrical characteristics of the unit fuel-cell is represented by a mathematical model described in [1]. Since the unit cell has a low output voltage and a small current rating, many unit cells are connected in series to form a stack structure so as to build up a reasonable terminal voltage. The voltage rating of the stack is determined by multiplying the unit cell voltage by the number of cells, while the current rating is determined by multiplying the unit cell current density by the cell area.

Table III shows the characteristic data for a commercial fuel cell stack, called a Nexa Power Module. The terminal voltage of the fuel cell stack is about 50V under the no load condition, while it is 26V under the full load condition.

Many computer simulations were carried out with PSCAD/EMTDC software to verify the operation of the proposed power conditioning system. The simulation model consists of a fuel-cell stack model, a 2-stage DC-DC converter, a grid-tied inverter, and a digital controller. The fuel-cell stack model and the digital controller were represented by user-defined models programmed in C-code, while the 2-stage DC-DC converter, the grid-tied inverter, and the 3-phase voltage source were represented by built-in models in the PSCAD/EMTDC software.

In order to confirm the voltage and current variations of the fuel cell according to the variation in the active power, a simulation scenario was selected as shown in Table IV. The active power varies in a step manner from 100W up to 1kW, and then down to 100W, while the reactive power varies from 0 up to 300Var, and then down to 0Var during 0~8 sec.

Fig. 13 shows the simulation results to verify the operation of the proposed system. Fig. 13(a) shows the operation voltage of the fuel cell, which changes according to the variation in the active power delivered to the grid.

Fig. 13(b) shows the operation current of the fuel cell, which changes according to the variation in the active power delivered to the grid similar to the case of the voltage variation.

Fig. 13(c) shows the tracking performance of the active power. It is clear that the transient phenomena can be stabilized within 1sec and that the steady-state tracking performance seems to be accurate. Fig. 13(d) shows the tracking performance of the reactive power. It is clear that the measured value

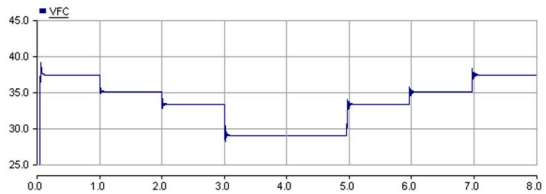

(a) Fuel-cell Operation Voltage.

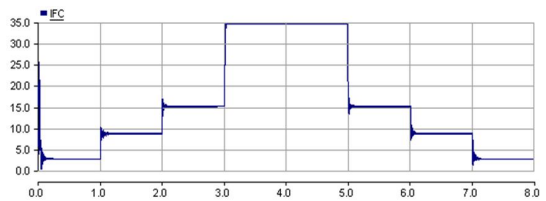

(b) Fuel-cell Operation Current.

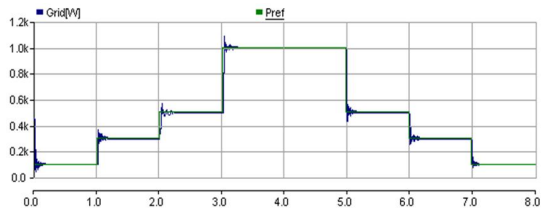

(c) Active-Power Control.

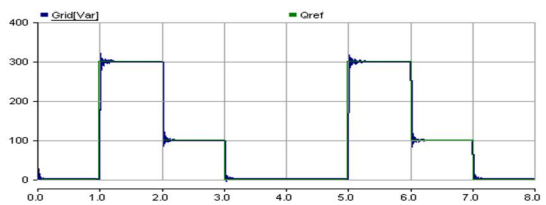

(d) Reactive-Power Control.

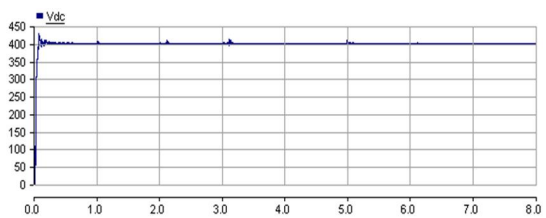

(e) DC Output Voltage Control.

Fig. 13. Simulation results of proposed system.

of the reactive power tracks the reference value accurately and that the transient phenomena is not so severe. Fig. 13(e) shows the tracking performance of the DC output voltage. The DC output voltage is maintained at 400V without severe transients.

VII. Experimental Work

A prototype of the proposed system was built and tested to confirm the feasibility of the hardware implementation as shown in Fig. 14. The fuel-cell power unit used in the experiment is a 1.2kW Ballard Nexa PEM Module. It has a monitoring system with a PC, which monitors the operation status of the fuel cell module through a communication link.

The 2-stage DC-DC converter was mounted on a rack together with the 3-phase inverter. The controller for the 2-stage DC-DC converter was designed and built with OP amps.

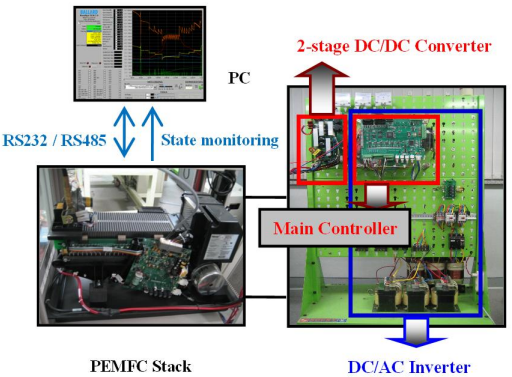

Fig. 14. Experiment Set-Up of Prototype.

TABLE V
Operation Scenario for Hardware Experiment

Time [s]	100	200	300	400	500	600	700	800
P [W]	100	300	500	1000	1000	500	300	100
Q [Var]	0	300	100	0	0	300	100	0

It adjusts the duty ratio of the 2-stage DC-DC converter to boosts the output voltage up to 400V. The boost converter stage was designed to operate with 30kHz of switching frequency and the LLC stage was designed to operate with 100kHz of switching frequency.

The controller for the grid-tied inverter was designed and built with a floating-point TMS320vc33-150 DSP and a EP1K100QC208 EPLD (Erasable Programmable Logic Device). The control board has 24ch of ADC, 4ch of DAC, 4ch of Digital Input, 4ch of Digital Output, 1module of Encoder pulse input, 1port of RS232, and 2ports of RS485.

The actual fuel-cell stack can not track the fast variation of the active power in the grid because the chemical reaction in the fuel cell stack is relatively much slower. In order to confirm safe and reliable operation, the duration of the active power variation was determined by 100sec in an actual experiment. A simulation scenario was selected as shown in Table V.

Fig. 15 shows the experimental results to verify the operation of the proposed system. Fig. 15(a) shows the operation voltage and current of a fuel cell module with 10V(A)/div. The time div was selected to be 100s, which is the same as the duration period of the active or reactive power. As the active power increases, the fuel cell voltage decreases while the fuel cell current increases. Fig. 15(b) shows that the measured active power tracks the reference value accurately without a severe transient.

Fig. 15(c) shows the output voltage and current variation of the fuel cell. The output current has the same variations as the active power while the capacitor voltage is maintained at 400V. This confirms that the DC-DC converter can accurately control the output voltage without a variation in the active power. Fig. 15(d) shows that the measured reactive power tracks the reference value accurately without a severe transient.

Fig. 16 shows the voltage-current characteristic curve for the fuel cell module used in the experiment. The no-load voltage of the fuel cell is about 50V and the terminal voltage goes

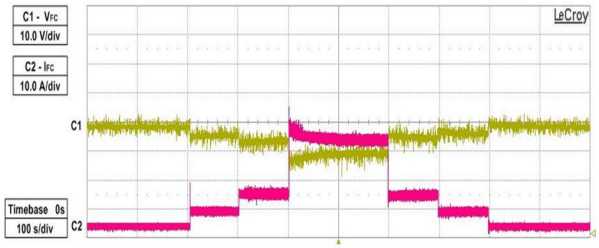

(a) Fuel-Cell Operation Voltage and Current.

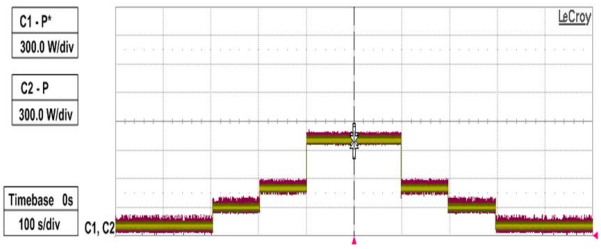

(b) Active-Power Control.

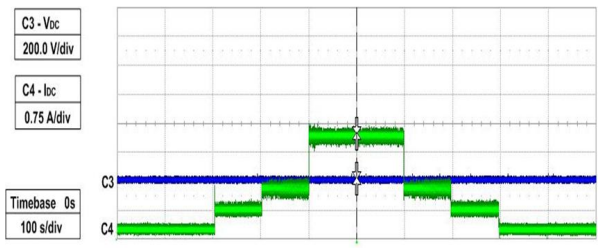

(c) DC Output Voltage and Current.

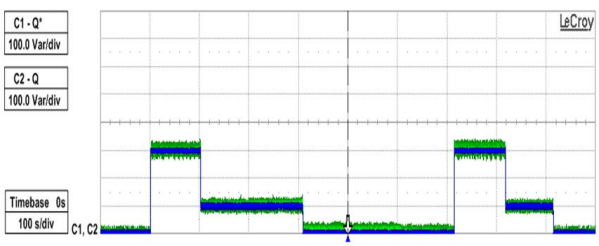

(d) Reactive-Power Control.

Fig. 15. Experimental Results of Hardware Prototype.

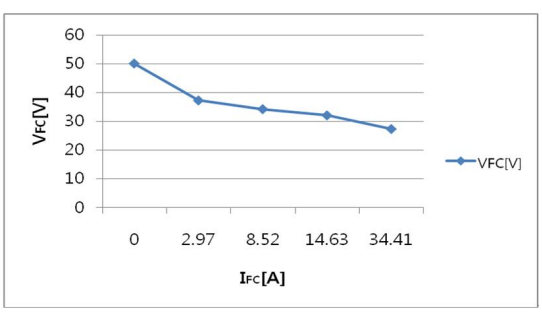

Fig. 16. Measured Fuel Cell Voltage and Current.

down while the output current increases and the active power increases. At an active power of 1kW, the fuel cell voltage is 27.3V, and the fuel cell current is 34.41A.

Fig. 17 shows the efficiency of the 2-stage DC-DC converter which was measured through experimentation. The efficiency was measured with respect to the lowest input voltage of

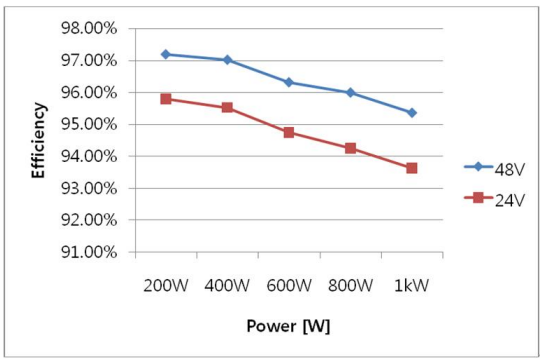

Fig. 17. Measured Efficiency of 2-Stage DC-DC Converter.

24V and the highest input voltage of 48V. The efficiency of the proposed converter is 93.5% when the input voltage is 24V and the output power is 1kW. Since the actual fuel cell voltage is 27.4V at an output of 1kW, it can be confirmed that the efficiency of the DC-DC converter is approximately 94%. Assuming that the efficiency of the grid-tied inverter is 97%, the total efficiency of the proposed power conditioning system could be about 91%.

VIII. Conclusion

This paper proposes a new grid-tied power conditioning system for fuel cell power generation. The proposed power conditioning system consists of a 2-stage DC-DC converter and a 3-phase inverter.

The 2-stage DC-DC converter is composed of a hard-switching boost converter cascaded with an unregulated LLC resonant converter. The fuel cell output voltage of 26-48V is boosted up to 80V by controlling the duty ratio of the hard-switching boost converter. The half-bridge LLC resonant converter boosts the input voltage of 80V up to 400V by operating a fixed duty ratio.

The operation of the proposed power conditioning system was verified through simulations with PSCAD/EMTDC software by checking the active and reactive power control capability. Based on the simulation results, a laboratory experimental set-up was built with a 1.2kW PEM fuel-cell stack to verify the feasibility of the hardware implementation.

The developed power conditioning system shows a high efficiency of 91%, which is very positive for commercialization. It can be used for implementing a micro-grid with fuel cell power generation.

Acknowledgment

The work was supported by a National Research Foundation of Korea Grant funded by the Korea Government (MEST), (NRF-2010-R1A5A003-2010-0026283).

References

[1] B. Yang, F. C. Lee, A. J. Zhang, and G. Huang, "LLC resonant converter for front end DC/DC conversion," in *Proc. APEC*, Vol. 2, pp. 1108-1112, 2002.

[2] T.-W. Lee, S.-H. Kim, Y.-H. Yoon, S.-J. Jang, and C.-Y. Won, "A 3 kW fuel cell generation system using the fuel cell simulator," in *Proc. Industrial Electronics*, Vol. 2, pp. 833-837, 2004.

[3] B. Bouneb, D. M. Grant, A. Cruden, and J. R. McDonald, "Grid connected inverter suitable for economic residential fuel cell operation," in *Proc. EPE*, p. 10, 2005.
[4] P. J. H. Wingelaar, J. L. Duarte, and M. A. M. Hendrix, "Dynamic characteristics of PEM fuel cells," in *Proc. PESC*, pp. 1635-1641, 2005.
[5] C. Wang and M. H. Nehrir, "Distributed generation applications of fuel cells," in *Proc. Power Systems Conference*, pp. 244-248, 2006.
[6] D. Polenov, H. Mehlich, and J. Lutz, "Requirements for MOSFETs in fuel cell power conditioning applications," in *Proc. EPE-PEMC*, pp. 1974-1979, 2006.
[7] A. K. Rathore, A. K. S. Bhat, and R. Oruganti, "A comparison of soft-switched DC-DC converters for fuel cell to utility interface application," in *Proc. PCC*, pp. 588-594, 2007.
[8] A. Mousavi, P. Das, and G. Moschopoulos, "A ZCS-PWM full-bridge boost converter for fuel-cell applications," in *Proc. APEC*, pp. 459-464, 2009.
[9] X. Yu, M. R. Starke, L. M. Tolbert, and B. Ozpineci, "Fuel cell power conditioning for electric power applications: a summary," in *Proc. IET*, Vol. 1, No. 5, pp. 643-656, 2007.
[10] S.-Y. Park, C.-L. Chen, and J.-S. Lai, "Wide range active and reactive power flow controller for a solid oxide fuel cell power conditioning system," in *Proc. APEC*, pp. 952-958, 2008.
[11] J.-M. Kwon, E.-H. Kim, B.-H. Kwon, and K.-H. Nam, "High-efficiency fuel cell power conditioning system with input current ripple reduction," *IEEE Trans. Ind. Electron.*, Vol. 56, No. 3, pp. 826-834, Mar. 2009.
[12] G. Hoogers, *FUEL CELL TECHNOLOGY HANDBOOK*, CRC Press, 2003.
[13] Texas Instrument Seminal Topics Slup170 - Estimating MOSFET parameters from the datasheet - http//focus.ti.com/lit/ml/slup170.pdf, 2002.

Jong-Kyou Jeong received his B.S. and M.S. in Electrical Engineering from Myongji University, Korea, in 2008 and 2010, respectively. He is currently working towards his Ph.D. at Myongji University. His current research interests include power electronic applications for custom power and distributed generation.

Byung-Moon Han (S'91-M'92-SM'00) received his B.S. in Electrical Engineering from Seoul National University, Korea, in 1976, and his M. S. and Ph.D. from Arizona State University in 1988 and 1992, respectively. He was with the Westinghouse Electric Corporation as a Senior Research Engineer in the Science and Technology Center. Currently he is a Professor in the Department of Electrical Engineering at Myongji University, Korea. His current research interests include power electronics applications for FACTS devices, custom power, and distributed generation.

Jun-Young Lee received his B.S. in Electrical Engineering from Korea University, CitySeoul, in 1993, and his M.S. and Ph.D. in Electrical Engineering from the Korea Advanced Institute of Science and Technology (KAIST), Taejon, Korea, in 1996 and 2001, respectively. Begining in 2001, he worked for four years as a Manager in the Plasma Display Panel Development Group, Samsung SDI where he was involved in circuit and product development. In 2005, he joined the School of Electronics and Computer Engineering, Dankook University, Chungnam, Korea, as a Senior Lecturer. His current research interests are in the areas of power electronics which include ac/dc power factor correction, converter topology design, converter modeling, soft switching techniques, display driving systems and liquid crystal display backlight units.

Nam-Sup Choi received his B.S. in Electrical Engineering from Korea University, Seoul, South Korea, in 1987. He received his M.S. and Ph.D. in Electrical Engineering from the Korean Advanced Institute of Science and Technology (KAIST), Taejon, South Korea, in 1989 and 1994, respectively. He is currently a Professor in the Division of Electrical Electronic Communication and Computer Engineering, Chonnam National University, Yeosu, South Korea. His current research interests include the modeling and control of power converters and systems.